Nanoscale

Cite this: *Nanoscale*, 2012, **4**, 6786

www.rsc.org/nanoscale

PAPER

Template-free approach to synthesize hierarchical porous nickel cobalt oxides for supercapacitors†

Jie Chang, Jing Sun,* Chaohe Xu, Huan Xu and Lian Gao

Received 4th July 2012, Accepted 31st August 2012
DOI: 10.1039/c2nr31725g

Nickel cobalt oxides with various Ni/Co ratios were synthesized using a facile template-free approach for electrochemical supercapacitors. The texture and morphology of the nanocomposites were characterized by powder X-ray diffraction (XRD), scanning electron microscopy (SEM), transmission electron microscopy (TEM) and Brunauer–Emmett–Teller analysis (BET). The results show that a hierarchical porous structure assembled from nanoflakes with a thickness of ~10 nm was obtained, and the ratio of nickel to cobalt in the nanocomposites was very close to the precursors. Cyclic voltammetry (CV) and galvanostatic charge and discharge tests were carried out to study the electrochemical performance. Both nickel cobalt oxides (Ni–Co–O-1 with Ni : Co = 1, Ni–Co-O-2 with Ni : Co = 2) outperform pure NiO and Co_3O_4. The Ni–Co–O-1 and Ni–Co–O-2 possess high specific capacities of 778.2 and 867.3 F g^{-1} at 1 A g^{-1} and capacitance retentions of 84.1% and 92.3% at 10 A g^{-1}, respectively. After full activation, the Ni–Co–O-1 and Ni–Co–O-2 could achieve a maximum value of 971 and 1550 F g^{-1} and remain at ~907 and ~1450 F g^{-1} at 4 A g^{-1}, respectively. Also, the nickel cobalt oxides show high capacity retention when fast charging.

1. Introduction

With the worsening of the environment and the depletion of fossil fuel, development of clean and high efficiency energy storage systems (lithium ion batteries, electrochemical supercapacitors, Ni–H batteries, *etc.*) has been put forward.[1] Among them, electrochemical supercapacitors have drawn considerable attention due to their fast charge–discharge properties and long cycle life.[2,3] There are mainly two kinds of supercapacitors based on the charge and discharge mechanism. The first are carbon based materials with large specific surface area, charging and discharging by an electric double layer mechanism. They usually exhibit high power density, excellent rate performance and long cycle life, but very low specific capacitance.[4–11] The second are pseudocapacitance materials (transition metal oxides (hydroxides)[12,13] and conductive polymers[14]), charging and discharging based on the redox reaction of active materials. They usually suffer from inferior rate performance, low utilization rate of active materials and poor cycle stability, though possessing extremely attractive theoretical capacitance values. To solve the problems, the real case of redox reaction in the active materials and electron and ion transmission during the charge and discharge process needs to be mentioned. It is generally accepted that the redox reaction between the active materials and the electrolyte ions occurs only in the thin surface layer of the active materials. The utilization rate of the active materials and the ion and electron transmission rates determine the specific capacitance and the rate performance of the supercapacitors, respectively. Hence, the construction of pseudocapacitance materials with large specific surface area, porosity and great electronic conductivity is highly preferred.

Owing to the large specific surface area and outstanding electronic conductivity of carbon nanotubes and graphene, they are usually incorporated into pseudocapacitance materials to enhance their performance.[15–25] An alternative way is to construct hierarchical porous structured pseudocapacitance materials. This kind of structure generally consists of one/two dimensional nanostructures featuring large specific surface area, pore volume and meso/macro pore distributions. The large specific surface area could guarantee more effective contact between the electrolyte ions and the active materials, hence raising their utilization rate. As the electrolyte buffering reservoirs and diverse diffusion channels, the rich pores could reduce the transport path and offer a robust retention of electrolyte ions to meet the demands of fast charge and discharge reactions.[26–37] For instance, nickel cobaltite nanowire assembled microspheres show a capacitance of 760 F g^{-1} and excellent rate performance.[30] Hierarchical microspheres based on α-$Ni(OH)_2$

The State Key Lab of High Performance Ceramics and Superfine Microstructure, Shanghai Institute of Ceramics, Chinese Academy of Sciences, 1295 Ding Xi Road, Shanghai 200050, China. E-mail: jingsun@mail.sic.ac.cn; Fax: +86 21 52413903; Tel: +86 21 52414301

† Electronic supplementary information (ESI) available: The morphology images, SAED patterns, nitrogen adsorption and desorption isotherms, pore size distribution curves and galvanostatic discharge curves of NiO and Co_3O_4 at various current densities in a potential range of 0–0.55 V. See DOI: 10.1039/c2nr31725g

nanosheets achieve a value of 1494 F g^{-1}.[28] Flower-like $Ni(OH)_2$ nanostructures could deliver a specific capacitance of 1715 F g^{-1} *etc.*[27] Unfortunately, the formation of a hierarchical porous structure usually needs the help of a structure directing agent (surfactant, soft or hard template). Either the introduction of large specific surface area carbon materials or the template will inevitably complicate the whole preparation process.

In this work, a series of hierarchical porous nickel cobalt oxides has been prepared without the introduction of any structure directing agent, which were self-assembled from two dimensional nanoflakes *via* solvothermal reaction and a subsequent annealing process. The nickel cobalt oxides exhibit high specific capacitance, and good rate performance and cycle stability making them promising pseudocapacitance materials for electrochemical supercapacitors.

2. Experimental

2.1 Synthesis of nickel cobalt oxides

All the chemicals were analytical grade and were used as received. The hierarchical porous nickel cobalt oxides were fabricated through a solvothermal and annealing process without the help of any structure directing agent. In a typical run, a certain amount of $Ni(NO_3)_2 \cdot 6H_2O$ and $Co(NO_3)_2 \cdot 6H_2O$ (total weight of nickel and cobalt nitrate hexahydrate was 2 g, ~6.87 mmol) was first dissolved in a mixture of *N*-methyl pyrrolidone (NMP 60 ml) and H_2O (5 ml). Then the mixture was heated to 180 °C and refluxed for 2 h. When cooled down to room temperature, the mixture was transferred to a 100 ml Teflon autoclave for solvothermal reaction at 180 °C for 6 h. Then the mixtures were filtered, washed and dried. Finally, the samples were collected after annealing for 6 h at 250 °C. To facilitate discussion, we term the nickel cobalt oxide as Ni–Co–O-1 and Ni–Co–O-2, with 1 and 2 denoting the molar ratio of Co^{2+} to Ni^{2+} in the precursors.

2.2 Characterization

Powder X-ray diffraction (XRD) analyses were performed on a Bruker D8 Advance diffractometer with Cu radiation at λ = 0.15418 nm. The morphologies and textures were tested on a scanning electron microscope (SEM JEOL S-4800) equipped with energy dispersive spectroscopy (EDS) and transmission electron microscopy (TEM JEOL 2100) equipped with selected area electron diffraction (SAED). The BET specific surface areas and pore size distributions were obtained from the N_2 adsorption and desorption isotherms recorded at 77 K on a Micrometrics ASAP 2010 BET analyzer.

2.3 Electrochemical measurement

The electrochemical properties of the products were investigated under a three electrode system, with a HgO/Hg electrode and platinum wire as the reference electrode and counter electrode, respectively, and 2 M KOH was used as electrolyte. For the preparation of the working electrode, the prepared powders were mixed with acetylene black and polyvinylidene fluoride (PVDF) at a weight ratio of 7 : 2 : 1 with the addition of a small amount of ethanol. Then the mixture was allowed to dry at 60 °C overnight. 4 mg of the prepared mixture was pressed onto nickel foam to make electrodes. Before the test, the working electrode was soaked for 2 h in the electrolyte. The cyclic voltammetry (CV) tests were conducted with a CHI 660D electrochemistry workstation. The galvanostatic charge and discharge tests were carried out on a LAND CT2001A cell measurement system.

3. Results and discussion

The powder XRD patterns of the prepared nickel cobalt oxides were displayed in Fig. 1. We found that pure cubic NiO (PDF#65-5745) or cubic Co_3O_4 (PDF#43-1003) was obtained when the precursor was individual $Ni(NO_3)_2 \cdot 6H_2O$ or $Co(NO_3)_2 \cdot 6H_2O$, respectively. For Ni–Co–O-1, cubic $NiCo_2O_4$ (PDF#20-0781) dominates accompanied by an amount of cubic NiO (the peak at ~63 deg can be attributed to the (200) plane of cubic NiO, the other peaks can be attributed to cubic $NiCo_2O_4$). For Ni–Co–O-2, all the diffraction peaks can be indexed to cubic $NiCo_2O_4$. However, this does not necessarily mean that cubic Co_3O_4 was absent from the nickel cobalt oxides due to the similarity in crystalline structure between $NiCo_2O_4$ and Co_3O_4.

The surface morphology of the nickel cobalt oxides was carefully observed by means of SEM. Fig. 2 displays the typical SEM images of Ni–Co–O-1 (a and b) and Ni–Co–O-2 (c and d), a hierarchical morphology was clearly observed. Both Ni–Co–O-1 and Ni–Co–O-2 are composed of interconnected thin nanoflakes (with a thickness ~10 nm) which loosely assembled and formed a hierarchical tremella-like structure with a lateral size of hundreds of nm. Also, the mesoporous characteristics are faintly visible from the fringe of the nanoflakes in Fig. 2b and d. The EDS results (Table 1) reveal that the molar ratio of Ni to Co of Ni–Co–O-1 and Ni–Co–O-2 are 1 : 1.08 and 1 : 2.09 which are very close to the starting molar ratio of nickel nitrate to cobalt nitrate.

To further view the microstructure of the hierarchical porous structure and the crystalline phase of the nickel cobalt oxides, TEM and SAED measurements were employed. The TEM images with different magnifications and SAED patterns of Ni–Co–O-1 (a–c) and Ni–Co–O-2 (d–f) are displayed in Fig. 3. Fig. 3a and d reveal the inner structure of the tremella-like nickel cobalt oxides; it can be seen that numerous thin nanoflakes assembled in all directions with many voids between them. The details of the nanoflakes are shown in Fig. 3b and e; a lot of

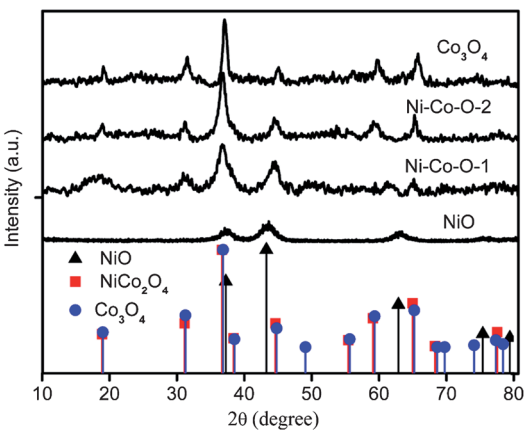

Fig. 1 Powder XRD patterns of the nickel cobalt oxides.

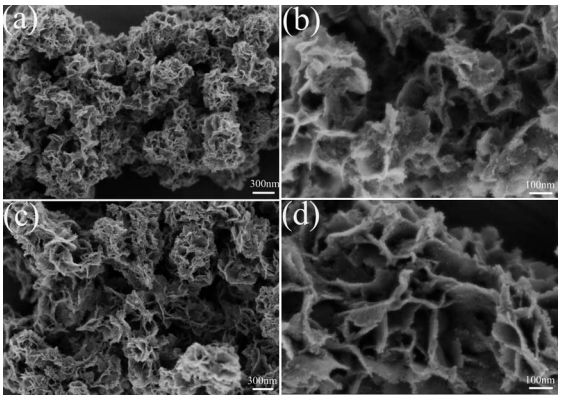

Fig. 2 Typical SEM images of Ni–Co–O-1 (a and b) and Ni–Co–O-2 (c and d).

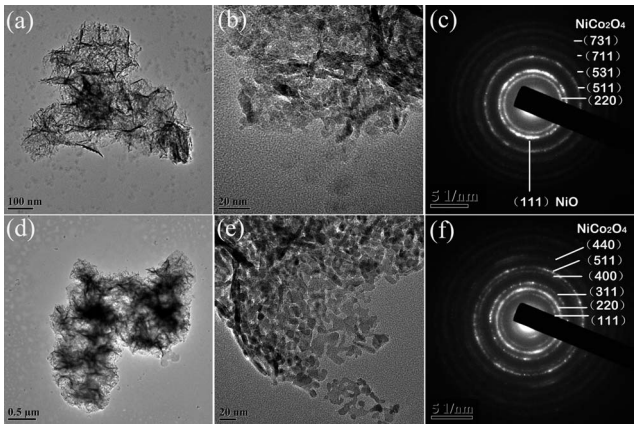

Fig. 3 TEM images and SAED pattern of Ni–Co–O-1 (a–c) and Ni–Co–O-2 (d–f).

mesopores existing in the nanoflakes can be distinctly seen, which matches well with the SEM results. All the SAED patterns of the nickel cobalt oxides show well-defined rings demonstrating their polycrystallinity. For Ni–Co–O-1 (Fig. 3c), the rings can be indexed to the (220), (511), (531), (711) and (731) planes of $NiCo_2O_4$ and the (111) plane for NiO. For Ni–Co–O-2 (Fig. 3f), all the rings can be indexed to the (111), (220), (311), (400), (511) and (440) planes of $NiCo_2O_4$. This is in good agreement with the XRD results. In the control experiments, the as-prepared NiO and Co_3O_4 also display a hierarchical porous structure and the SAED patterns (Fig. S1†) show their pure phases.

Generally, specific surface area, pore diameter and pore volume all play a part in determining the electrochemical properties of the active materials. The surface area and pore size distribution analysis were investigated using nitrogen adsorption and desorption isotherms. Fig. 4 and S2† show the nitrogen adsorption and desorption isotherms and pore size distribution curves of the nickel cobalt oxides. All the isotherms are similar to each other in form. In the medium relative pressure region, the adsorbed N_2 increases steadily with the increase of relative pressure due to capillary condensation and multilayer adsorption in the mesopores. The sharp climb in the high pressure region can be attributed to adsorption in the voids among the nanoflakes. The pore size distribution curves disclose the coexistence of mesopores and macropores. Table 1 gives the important structural parameters derived from the nitrogen adsorption and desorption isotherms of the prepared nanocomposites. The specific surface areas of Ni–Co–O-1 and Ni–Co–O-2 are 153.2 and 113.2 $m^2\ g^{-1}$, respectively. Both the average pore diameter and total pore volume are increased in comparison with pure NiO or Co_3O_4. The rich pores and large pore volume (0.5080 and 0.4429 $cm^3\ g^{-1}$) could greatly ensure that enough electrolyte ions

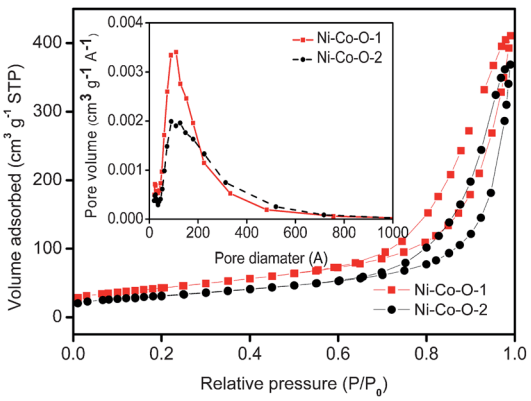

Fig. 4 Nitrogen adsorption and desorption isotherms of Ni–Co–O-1 and Ni–Co–O-2, inset was pore size distribution curves.

have easy access to the surface of the active materials. It is noteworthy that the Faradaic reactions causing the pseudocapacitance usually only occurred in a very thin surface layer of the active materials. The as-prepared hierarchical structure meets the basic requirements for high performance electrochemical supercapacitors.

Cyclic voltammetry (CV) tests were performed in a potential range of 0–0.65 V (*vs.* Hg/HgO) at a scan rate of 10 mV s^{-1} using 2 M KOH as electrolyte under a three electrode system, with a HgO/Hg electrode and platinum wire as the reference electrode and counter electrode, respectively. All the CV curves exhibit a pair of cathodic and anodic peaks, revealing their pseudocapacitive characteristics. It is generally accepted that the specific capacitance of the sample is directly proportional to the area of

Table 1 Physical properties of the nickel cobalt oxides

Samples	Specific surface area ($m^2\ g^{-1}$)	Average pore diameter (nm)	Total pore volume ($cm^3\ g^{-1}$)	Atomic ratio of Ni/Co
NiO	149.6	9.6	0.3593	Pure NiO
Ni–Co–O-1	153.2	13.2	0.5080	1 : 1.08
Ni–Co–O-2	113.2	15.6	0.4429	1 : 2.09
Co_3O_4	72.8	12.8	0.2327	Pure Co_3O_4

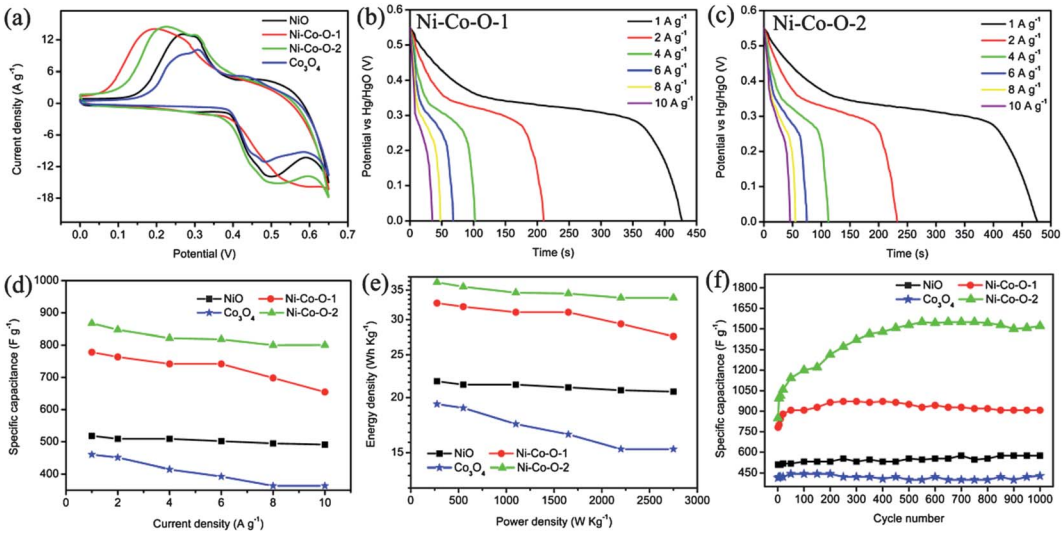

Fig. 5 Electrochemical characterization of nickel cobalt oxides. (a) CV curves at 10 mV s^{-1} in a potential range of 0–0.65 V, galvanostatic discharge curves of Ni–Co–O-1 (b) and Ni–Co–O-2 (c) at various current densities in a potential range of 0–0.55 V, (d) the specific capacitance of nickel cobalt oxide at various current densities, (e) Ragone plots of nickel cobalt oxides and (f) cyclic performance of nickel cobalt oxides at 4 A g^{-1}.

the CV curves covered. Evidently, Ni–Co–O-1 and Ni–Co–O-2 present larger specific capacitances than NiO and Co_3O_4, deduced from the area of the CV curves covered. To evaluate the electrochemical performance in detail, galvanostatic charge and discharge tests were conducted. Fig. 5(b and c) show the galvanostatic discharge curves of Ni–Co–O-1 (b) and Ni–Co–O-2 (c) at various current densities. The discharge curves exhibit a plateau at 0.25–0.35 V which is characteristic of pseudocapacitance, hence verifying the CV results. For comparison, the galvanostatic discharge curves of NiO and Co_3O_4 were displayed in Fig. S3.† The specific capacitances at various current densities (Fig. 5d) were calculated based on the discharge curves. Firstly, it can be seen that the specific capacitance of the nickel cobalt oxides slightly decreases with the increase of current densities. This could be explained by a pseudocapacitance mechanism; some ions have not participated in the Faradaic redox reaction due to the slow diffusion rate and electron transfer rate at higher current density. For Ni–Co–O-1, the specific capacitance is 778.2 F g^{-1} at 1 A g^{-1}, and 654.5 F g^{-1} at 10 A g^{-1}, which is *ca.* 84.1% of that at 1 A g^{-1}. For Ni–Co–O-2, the specific capacitance is 867.3 F g^{-1} at 1 A g^{-1}, the capacitance retention at 10 A g^{-1} is 92.3% (*ca.* 800.4 F g^{-1}). The corresponding values for NiO and Co_3O_4 were 518.2 F g^{-1}, 490.9 F g^{-1}, 94.7% and 460.0 F g^{-1}, 363.6 F g^{-1}, 79.0%, respectively. The overall capacitance retention is superior to most previous reports,[18,28,29,38] and we can infer that the remarkable rate performance concerns their hierarchical porous structure much more. Secondly, the nickel cobalt oxides possess higher capacitance than pure NiO or Co_3O_4. Considering the similarity in structure and the BET results, we speculate that the disparity in capacitance can be mainly attributed to the composition difference and pore volume. The presence of $NiCo_2O_4$ in the nickel cobalt oxides greatly boosts the electrochemical performance due to its much better electronic conductivity and electrochemical activity.[39] Moreover, the large pore volume could offer a robust retention of K^+ to meet the requirements of fast Faradaic reaction.

Ragone plots derived from the discharge curves are shown in Fig. 5e. In a potential range of 0.55 V, Ni–Co–O-1 and Ni–Co–O-2 deliver energy densities of 32.69 and 36.44 W h kg^{-1} at a power density of 275 W kg^{-1}, respectively. The corresponding

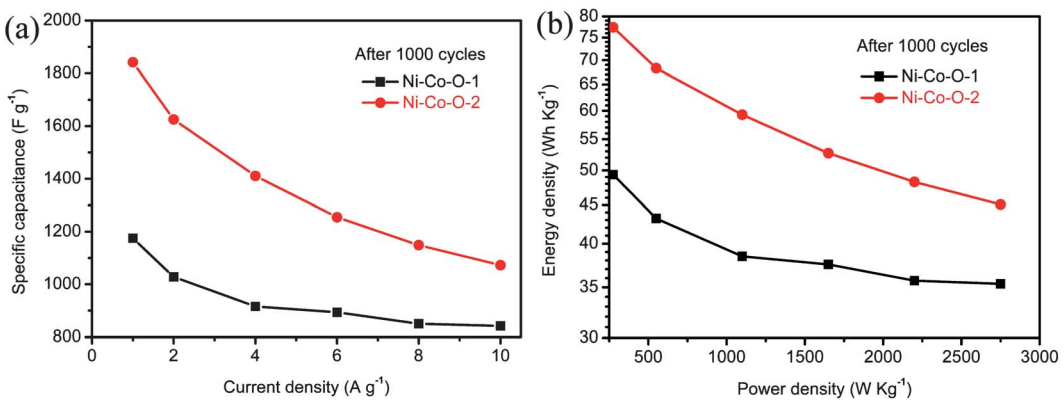

Fig. 6 (a) The specific capacitance of Ni–Co–O-1 and Ni–Co–O-2 at various current densities, (b) Ragone plots of Ni–Co–O-1 and Ni–Co–O-2.

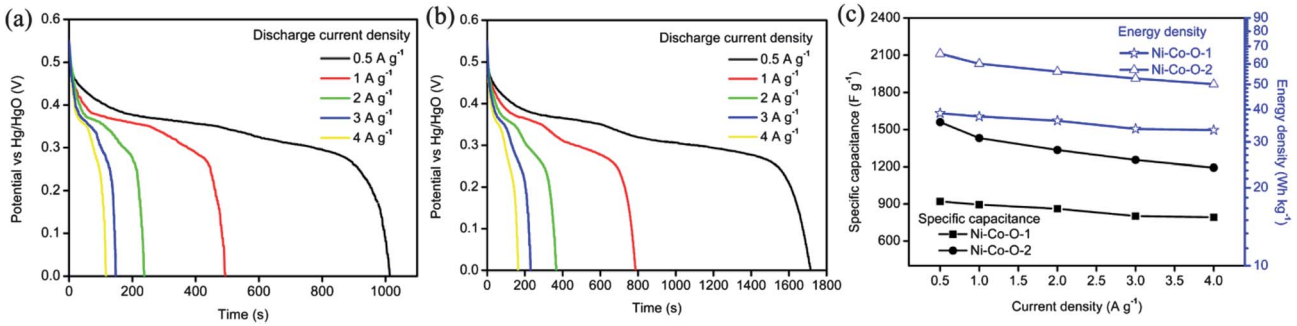

Fig. 7 The fast charge and low discharge characterization. The discharge curves of Ni–Co–O-1 (a) and Ni–Co–O-2 (b) at various discharge current densities with a fast charge current density of 10 A g^{-1}. (c) The discharge specific capacitance *versus* the various discharge current densities and the Ragone plots derived from the discharge curves charged at 10 A g^{-1}.

values are 27.5 and 33.61 W h kg^{-1} at 2750 W kg^{-1}. As long cycle life is extremely important for supercapacitors, the cycle stability was tested by means of galvanostatic charge and discharge at a current density of 4 A g^{-1} (Fig. 5f). Interestingly, the specific capacitance of Ni–Co–O-1 and Ni–Co–O-2 has a sharp increase in the first hundred cycles, and can reach a maximum of 971 and 1550 F g^{-1}, respectively. Then, both decrease slightly compared with the maximum value and can remain at ~907 and ~1450 F g^{-1}, respectively, in the last hundred cycles. A similar phenomenon was also reported by other groups.[18,38] The penetration of electrolyte ions and the gradual activation of the active materials may be responsible for the increase of the specific capacitance in the first several hundred cycles. In the control experiment, NiO and Co_3O_4 also display a relatively small increase in specific capacitance after several charge and discharge cycles.

Because of the large increase of capacitance during the cycles, it is necessary to study the real case after sufficient activation. Fig. 6 displays the capacitance performance of Ni–Co–O-1 and Ni–Co–O-2 at various current densities after 1000 cycles. It can be seen that the specific capacitance of Ni–Co–O-1 and Ni–Co–O-2 can achieve extremely high values of 1175 and 1841 F g^{-1} at 1 A g^{-1}. The corresponding values are 842 and 1072 F g^{-1} at 10 A g^{-1}. These values are much higher than most previous reports on nickel cobalt oxides.[18,30,38,39] The Ragone plots (Fig. 6b) demonstrate that the Ni–Co–O-1 and Ni–Co–O-2 could deliver an energy density of 49.4 and 77.4 W h Kg^{-1} at a power density of 275 W Kg^{-1} after 1000 cycles. Even at 2750 W Kg^{-1}, high values of 35.4 and 45.1 W h kg^{-1} are maintained.

Considering the situation that sometimes we need quick collection of energy in real applications, the fast charge and low discharge properties were investigated. Therefore, the nickel cobalt oxide electrodes were first charged at a high current density of 10 A g^{-1}, then discharged at a series of lower current densities. Based on the discharge curves of Ni–Co–O-1 (Fig. 7a) and Ni–Co–O-2 (Fig. 7b), the average specific capacitance and energy density were calculated. As depicted in Fig. 7c, the specific capacitance and energy density of Ni–Co–O-1 were slightly influenced by the discharge current density (921 to 795 F g^{-1} and 38.7 to 33.3 W h kg^{-1} with the discharge current density from 0.5 to 4 A g^{-1}). The specific capacitance discharged at 4 A g^{-1} with a charge current density of 10 A g^{-1} is about 86.4% of that charged at 4 A g^{-1}. However, for Ni–Co–O-2, the specific capacitance and energy density at 0.5 and 4 A g^{-1} were 1560 F g^{-1}, 65.5 W h kg^{-1} and 1192 F g^{-1}, 50.1 W h kg^{-1}, respectively. The capacitance retention is about 81.7% from a charge density of 4 to 10 A g^{-1}. In other words, the electrodes based on nickel cobalt oxide could possess high capacity retention when fast charging.

4. Conclusion

In summary, nickel cobalt oxides with a hierarchical porous structure were successfully prepared using a template-free method. The unique structure could greatly raise the utilization rate of active materials and guarantee the quick transmission of electrolyte ions, due to the large specific surface area, meso/macro pore structure and large pore volumes. The nickel cobalt oxides show much better capacitance performance than pure Co_3O_4 and NiO probably due to the formation of $NiCo_2O_4$, making them promising electrode materials for electrochemical supercapacitors.

Acknowledgements

This work is supported by the National Basic Research Program of China (2012CB932303) and the National Natural Science Foundation of China (Grant no. 51072215 and 51172261).

References

1 C. Liu, F. Li, L. P. Ma and H. M. Cheng, *Adv. Mater.*, 2010, **22**, E28.
2 Y. Zhang, H. Feng, X. B. Wu, L. Z. Wang, A. Q. Zhang, T. C. Xia, H. C. Dong, X. F. Li and L. S. Zhang, *Int. J. Hydrogen Energy*, 2009, **34**, 4889–4899.
3 G. Wang, L. Zhang and J. Zhang, *Chem. Soc. Rev.*, 2012, **41**, 797.
4 L. L. Zhang and X. S. Zhao, *Chem. Soc. Rev.*, 2009, **38**, 2520–2531.
5 P. Sharma and T. S. Bhatti, *Energy Convers. Manage.*, 2010, **51**, 2901–2912.
6 H. M. Sun, L. Y. Cao and L. H. Lu, *Energy Environ. Sci.*, 2012, **5**, 6206–6213.
7 J. T. Zhang, J. W. Jiang, H. L. Li and X. S. Zhao, *Energy Environ. Sci.*, 2011, **4**, 4009–4015.
8 C. X. Guo and C. M. Li, *Energy Environ. Sci.*, 2011, **4**, 4504–4507.
9 Y. Kou, Y. H. Xu, Z. Q. Guo and D. L. Jiang, *Angew. Chem., Int. Ed.*, 2011, **50**, 8753–8757.
10 S. W. Lee, B. S. Kim, S. Chen, Y. Shao-Horn and P. T. Hammond, *J. Am. Chem. Soc.*, 2009, **131**, 671–679.
11 D.-W. Wang, F. Li, M. Liu, G. Q. Lu and H.-M. Cheng, *Angew. Chem., Int. Ed.*, 2008, **47**, 373–376.
12 W. Wei, X. Cui, W. Chen and D. G. Ivey, *Chem. Soc. Rev.*, 2011, **40**, 1697.
13 V. Khomenko, E. Raymundo-Pinero and F. Beguin, *J. Power Sources*, 2006, **153**, 183–190.

14 G. A. Snook, P. Kao and A. S. Best, *J. Power Sources*, 2011, **196**, 1–12.
15 X. Huang, X. Y. Qi, F. Boey and H. Zhang, *Chem. Soc. Rev.*, 2012, **41**, 666–686.
16 S. B. Yang, X. L. Wu, C. L. Chen, H. L. Dong, W. P. Hu and X. K. Wang, *Chem. Commun.*, 2012, **48**, 2773–2775.
17 H. L. Wang, H. S. Casalongue, Y. Y. Liang and H. J. Dai, *J. Am. Chem. Soc.*, 2010, **132**, 7472–7477.
18 H. W. Wang, Z. A. Hu, Y. Q. Chang, Y. L. Chen, H. Y. Wu, Z. Y. Zhang and Y. Y. Yang, *J. Mater. Chem.*, 2011, **21**, 10504–10511.
19 I. Muylaert, J. Musschoot, K. Leus, J. Dendooven, C. Detavernier and P. Van der Voort, *Eur. J. Inorg. Chem.*, 2012, 251–260.
20 F. Huang and D. Chen, *Energy Environ. Sci.*, 2012, **5**, 5833.
21 W. H. Shi, J. X. Zhu, D. H. Sim, Y. Y. Tay, Z. Y. Lu, X. J. Zhang, Y. Sharma, M. Srinivasan, H. Zhang, H. H. Hng and Q. Y. Yan, *J. Mater. Chem.*, 2011, **21**, 3422–3427.
22 Q. T. Qu, S. B. Yang and X. L. Feng, *Adv. Mater.*, 2011, **23**, 5574.
23 K. Wang, P. Zhao, X. M. Zhou, H. P. Wu and Z. X. Wei, *J. Mater. Chem.*, 2011, **21**, 16373–16378.
24 H. L. Wang, Q. L. Hao, X. J. Yang, L. D. Lu and X. Wang, *Nanoscale*, 2010, **2**, 2164–2170.
25 J. J. Xu, K. Wang, S. Z. Zu, B. H. Han and Z. X. Wei, *ACS Nano*, 2010, **4**, 5019–5026.
26 C. Yuan, L. Hou, L. Yang, D. Li, L. Shen, F. Zhang and X. Zhang, *J. Mater. Chem.*, 2011, **21**, 16035.
27 H. Jiang, T. Zhao, C. Z. Li and J. Ma, *J. Mater. Chem.*, 2011, **21**, 3818–3823.
28 J. W. Lee, J. M. Ko and J. D. Kim, *J. Phys. Chem. C*, 2011, **115**, 19445–19454.
29 L. B. Kong, J. W. Lang, M. Liu, Y. C. Luo and L. Kang, *J. Power Sources*, 2009, **194**, 1194–1201.
30 H. L. Wang, Q. M. Gao and L. Jiang, *Small*, 2011, **7**, 2454–2459.
31 Z.-A. Hu, Y.-L. Xie, Y.-X. Wang, H.-Y. Wu, Y.-Y. Yang and Z.-Y. Zhang, *Electrochim. Acta*, 2009, **54**, 2737–2741.
32 X. H. Lu, D. Z. Zheng, T. Zhai, Z. Q. Liu, Y. Y. Huang, S. L. Xie and Y. X. Tong, *Energy Environ. Sci.*, 2011, **4**, 2915–2921.
33 S. Dong, X. Chen, L. Gu, X. Zhou, L. Li, Z. Liu, P. Han, H. Xu, J. Yao, H. Wang, X. Zhang, C. Shang, G. Cui and L. Chen, *Energy Environ. Sci.*, 2011, **4**, 3502.
34 D. W. Wang, F. Li and H. M. Cheng, *J. Power Sources*, 2008, **185**, 1563–1568.
35 S. B. Ma, K. W. Nam, W. S. Yoon, X. Q. Yang, K. Y. Ahn, K. H. Oh and K. B. Kim, *Electrochem. Commun.*, 2007, **9**, 2807–2811.
36 R. Liu, J. Duay and S. B. Lee, *ACS Nano*, 2011, **5**, 5608–5619.
37 R. Liu and S. B. Lee, *J. Am. Chem. Soc.*, 2008, **130**, 2942–2943.
38 G. X. Hu, C. H. Tang, C. X. Li, H. M. Li, Y. Wang and H. Gong, *J. Electrochem. Soc.*, 2011, **158**, A695–A699.
39 T. Y. Wei, C. H. Chen, H. C. Chien, S. Y. Lu and C. C. Hu, *Adv. Mater.*, 2010, **22**, 347.